JOURNAL OF AIRCRAFT
Vol. 46, No. 3, May–June 2009

Plasma Flaps and Slats: An Application of Weakly Ionized Plasma Actuators

Chuan He[†] and Thomas C. Corke[*]
University of Notre Dame, Notre Dame, Indiana 46556
and
Mehul P. Patel[‡]
Orbital Research, Inc., Cleveland, Ohio 44103

DOI: 10.2514/1.38232

The experimental validation of an application of weakly-ionized plasma actuators for improved aerodynamic performance of multi-element wings and wings with movable control surfaces is presented. Two spanwise arrays of plasma actuators, configured to produce a wall-jet effect, were applied on the suction surface of a two-dimensional NACA 0015 wing model, one at the leading edge and the other near the trailing edge to mimic the effects of a wing leading-edge slat and a trailing-edge flap, respectively. Flow control tests were conducted at chord Reynolds numbers, corrected for blockage, of 0.217×10^6 and 0.307×10^6 in a low-speed wind tunnel at the University of Notre Dame. The leading-edge-separation control resulted in an increase in both the maximum lift coefficient and the stall angle of attack and a lift-to-drag improvement of as much as 340%. An optimum frequency was found to exist for unsteady excitation of the leading-edge separation. Under this condition, the power to the actuator was estimated to be only 2 W. The trailing-edge actuator was found to produce the same effect as a plain trailing-edge flap. This included a uniform shift at all angles of attack of the lift coefficient and a shift toward higher lift coefficients of the drag bucket. In addition, there was a slight decrease in the minimum drag coefficient. The obvious advantages of this approach are its simplicity, as there are no moving parts, and its lack of hinge gaps, which add drag. An example of their use as ailerons for roll control produces a comparable roll moment coefficient to a sample general aviation aircraft.

Nomenclature

C_D	=	drag coefficient
C_L	=	lift coefficient
$C_{\mathcal{L}}$	=	roll moment coefficient
$C_{\mathcal{L}_{\delta a}}$	=	roll moment derivative
C_{L_α}	=	lift coefficient angle of attack slope, $dC_L/d\alpha$
c	=	wing chord
c_f	=	equivalent plain flap chord
D	=	drag force
f	=	excitation frequency of unsteady plasma actuator, Hz
L	=	lift force
$\mathcal{L}$	=	roll moment
L_{sep}	=	streamwise extent of separation zone
q	=	dynamic pressure
Re_c	=	Reynolds number based on chord length and freestream velocity
St	=	Strouhal number, fc/U_∞
U_∞	=	freestream velocity measured at entrance to test section
u'	=	root mean square of streamwise velocity fluctuations
V	=	plasma actuator voltage
x, y	=	axial coordinates
α	=	angle of attack
α_{0L}	=	zero-lift angle of attack
$\Delta_{\alpha 0L}$	=	change in zero-lift angle of attack

Subscripts

max	=	maximum value
$p-p$	=	peak-to-peak level
s	=	condition at stall

Presented as Paper 2127 at the 2nd AIAA Flow Control Conference, Portland, Oregon, 28 June–1 July 2004; received 23 April 2008; revision received 12 September 2008; accepted for publication 17 September 2008.

[*]Clark Chair Professor, Center for Flow Physics and Control, Aerospace and Mechanical Engineering Department. Associate Fellow AIAA.
[†]Graduate Assistant, Center for Flow Physics and Control, Aerospace and Mechanical Engineering Department.
[‡]Director, Aerodynamics Group. Member AIAA.

I. Introduction

THE maximum lift and stall characteristics of a wing affect many performance aspects of aircraft, including takeoff and landing distance, maximum and sustained turn rates, climb and glide rates, and flight ceiling [1]. On a two-dimensional wing, the maximum achievable lift is ultimately limited by the ability of the flow to negotiate regions with an adverse pressure gradient. When it cannot, the flow separates. At large angles of attack, this occurs at the leading edge.

One solution to prevent leading-edge separation is to reduce the severity of the pressure peak ordinarily associated with high angles of attack. This is the principal effect of a leading-edge flap. An example is a Krueger flap, which consists of a hinged surface on the lower side of the wing that can extend out and ahead of the wing leading edge. A slotted leading-edge flap (slat) is the leading-edge equivalent of a slotted trailing-edge flap. It works by allowing air from the high-pressure lower surface to flow to the upper surface to add momentum to the boundary layer and prevent flow separation.

Conventional multi-element wings and wings with movable control surfaces, such as the leading-edge slats and trailing-edge flaps that contain gap regions, are a major source of airframe noise and vibration, especially at high deflection angles. Most of the noise originates from the separated flow in the gap regions. It is also known that the hinge gaps contribute to the form drag component of the viscous drag on the wing. To improve the aerodynamic performance of the wing, it is desirable to either completely replace the traditional moving surfaces with hingeless control surfaces or limit the deflections of moving surfaces without compromising the wing's performance. Both these alternatives necessitate other approaches for controlling flow separation over the surface of the wing.

This work is focused on the application of weakly ionized plasma actuators to control flow separation on the wing in a manner that can potentially replace the leading-edge slat and trailing-edge flap of a wing with an array of plasma actuators on the leading edge (plasma slat configuration) and on the trailing edge (plasma flap configuration), respectively.

Eliminating the hinge gaps will have a direct effect on the form drag component of the viscous drag on the wing. By present estimates used in the wing and tail design, this would result in a 10% drag decrease [1]. The hinge gap is also a source of radar wave reflection; hence, by eliminating the gap, the wing radar signature could be significantly improved.

In the ultimate application of the plasma actuators on wings, a "virtual section shape" would come about by strategically tiling the surface of a generic wing shape with plasma actuators that would be designed to correct for local flow separations or locally augment the aerodynamic forces. This could lead to choices that are based on considerations other than aerodynamics, such as internal volume or strength-to-weight ratio. The aerodynamics of the wing might then be varied according to a flight plan, for example, high lift for takeoff and landing, and a virtual drag bucket at the design C_L for efficient cruise and endurance.

A. Single Dielectric Barrier Discharge Plasma Actuators

The single dielectric barrier discharge (SDBD) plasma actuator consists of two electrodes that are separated by a dielectric material. One of the electrodes is exposed to the air. The other electrode is fully covered by the dielectric material. A schematic illustration of the actuator configuration used in this work is shown in Fig. 1. A high-voltage ac input is supplied to the electrodes. When the ac voltage amplitude is large enough, the air ionizes in the region of the largest electric potential. This generally begins at the edge of the electrode that is exposed to the air and spreads out over the area projected by the covered electrode. The location of the plasma is denoted in Fig. 1.

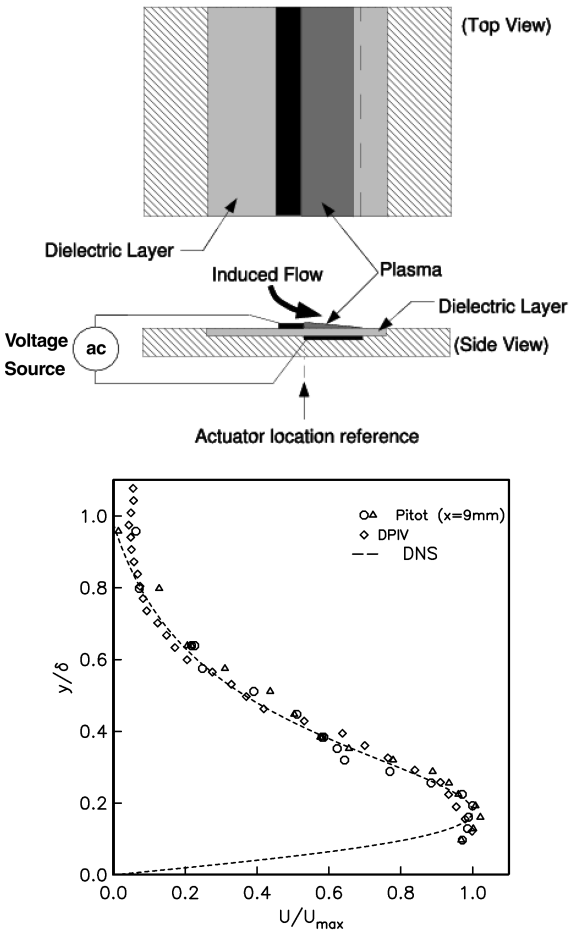

Fig. 1 Schematic drawing of SDBD plasma actuator and normalized mean velocity distribution produced by this actuator arrangement [14].

The process of ionizing the air in this configuration is classically known as a single dielectric barrier discharge [2]. A recent general review of SDBD plasma actuators for flow control was given by Corke et al. [3]. The ionized air (plasma) in the presence of an electric field gradient produces a body force on the ambient air [4]. The body force per volume of plasma is a vector, which is given as [4]

$$\boldsymbol{f}_b^* = -\left(\frac{\varepsilon_0}{\lambda_D^2}\right)\varphi \boldsymbol{E} \tag{1}$$

where φ is the electric potential, $\boldsymbol{E}$ is the electric field, λ_D is the is the Debye length, and ε_0 is the permittivity of air.

The formation of the plasma is a dynamic process that varies in time and space during the ac cycle [2]. Orlov et al. [5,6] developed a lumped circuit model from which the space–time-dependent body force can be computed. This model provides insight into the dependence of the body force on the ac frequency and amplitude, wave form shape, and electrode geometry.

This body force vector can be tailored through the design of the electrode and dielectric arrangement, which control the spatial electric field. The body force representation is also a convenient form to incorporate the effect of the actuators in Navier–Stokes (NS) simulations of the flowfield. Such NS simulations have been used to design and optimize different plasma actuator arrangements [7–9]. Other actuator optimizations come from the choice of the ac time series shape, which controls the amount and duration of the plasma.

The SDBD plasma actuators are low-power devices, with typical ac cycle-integrated power levels of approximately 20 W/ft of actuator span. They can be operated either in a "quasi-steady" or unsteady manner. In the quasi-steady operation, the typical input ac frequency of 5–20 kHz is often well above the fluid response frequency; therefore, the flow senses an effectively constant body force. In the unsteady operation, the higher-driving ac frequency is switched on and off at lower frequencies down to a fraction of a hertz. The unsteady operation can be used to excite fluid instabilities that act as a fluid amplifier to produce a larger flow effect. In the unsteady approach, very short duty cycles are possible, which reduces the actuator power significantly. For example, results in this paper were obtained with a 10% duty cycle that effectively reduced the power by 90% over the steady operation and provided as good or better overall flow control.

Examples of different applications that have used SDBD plasma actuators for aerodynamic control on wings include lift control [10–12] and leading-edge-separation control [13–16]. Other recent experiments have used SDBD plasma actuators for separation control in turbine-blade simulations [17–20].

II. Experimental Setup

A. Wind Tunnel

The experiments were conducted in one of the subsonic wind tunnels at the Center for Flow Physics and Control at the Hessert Laboratory of the University of Notre Dame. The facility is an open-return draw-down wind tunnel with a 0.421 m (1.39 ft) square cross section by 1.8-m-long (6-ft-long) test section. The tunnel consists of a removable inlet with a series of 12 screens followed by a 24:1 contraction that attaches to the test section. The turbulence level in the test section, u'/U_∞, over the range of velocities used in the experiment is approximately 0.08%.

The test section is equipped with a clear Plexiglas side wall that allows optical access to view the model. The back wall of the test section has removable panels to allow access into the test section.

The airfoil used in the study was mounted on the support sting of a lift–drag force balance. The force balance was mounted on the top of the test section. A schematic of the force balance and a photograph of it with the airfoil in the test section is shown in Fig. 2. Further details of the force balance are given by Mueller [21]. The airfoil was suspended between splitter plates that were attached to the ceiling and floor of the test section. The splitter plates were designed to

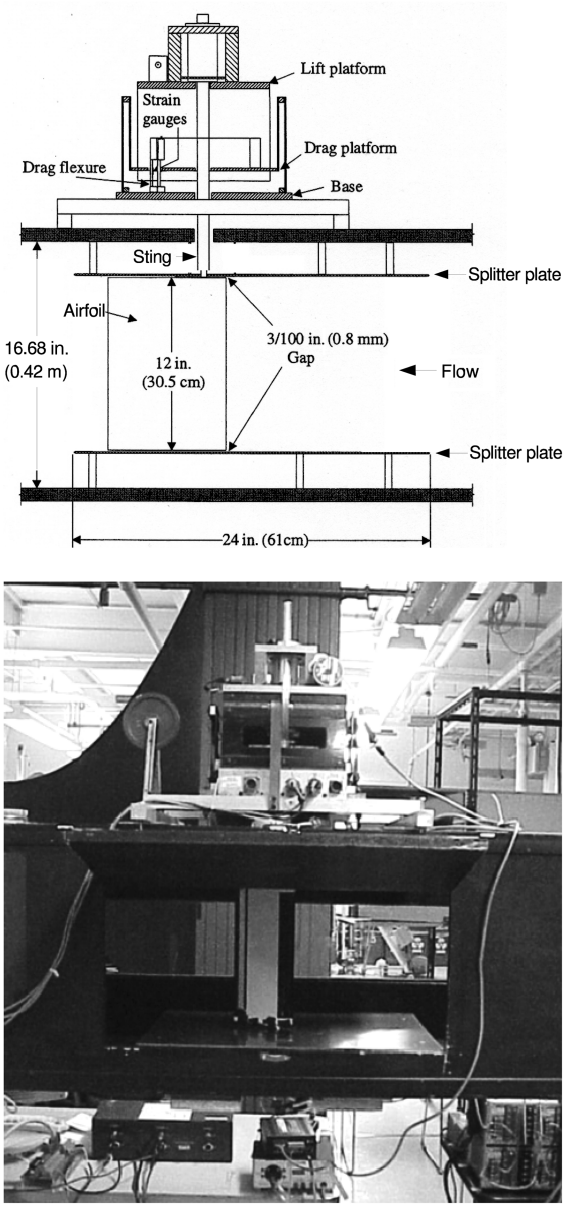

Fig. 2 Schematic of airfoil and force balance arrangement and corresponding photograph in wind-tunnel test section.

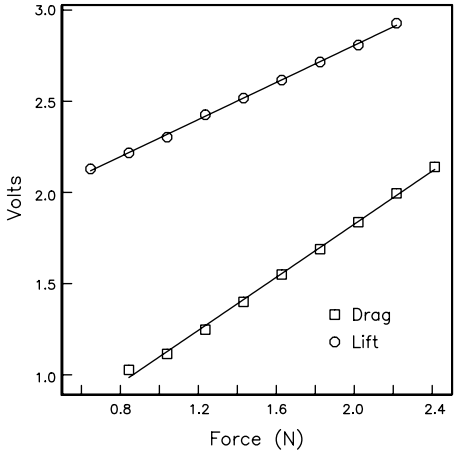

Fig. 3 Sample lift and drag force calibration of voltage output from force balance used in experiments.

produce a two-dimensional flow around the airfoil. A hole in the ceiling end plate accommodated the sting supporting the airfoil. A hole in the floor end plate allowed access for the actuator wiring. This hole was aligned with the support sting so that it would not interfere with angular positioning of the airfoil when setting different angles of attack. A stepper motor on the force balance drove the angular position of the support sting. Its motion was controlled by the data acquisition computer using software.

The force balance consists of independent lift and drag platforms. The lift platform is supported on the drag platform by two vertical plates that flex only in the lift direction. The drag platform is supported by two plates that flex only in the drag direction and hang from two more vertical plates attached to the fixed base of the force balance. Both the lift and drag platforms are connected to separate flexures on which foil strain-gauge bridges are mounted. The strain-gauge bridges provide voltage outputs proportional to the respective lift and drag forces. The voltages were amplified using custom-designed operational amplifier circuits that minimized offset drift and sensitivity to external electronic noise.

Calibration of the force balance was done by applying known weights to a cable pulley system attached to the support sting. Calibration was performed with the model attached. An example of the force calibration is shown in Fig. 3. The curve through the calibration points is the result of a straight line fit that was used to convert the force balance voltages to lift and drag values. The standard deviation of the linear fits were 0.011 N for lift and 0.023 N for drag. Based on a mean force of 1.6 N, the average uncertainty in the force measurements was 0.63% in lift and 0.90% in drag.

The experiment was controlled by a digital computer with a programmable A/D converter and digital input–output (DIO) interface. The minimum voltage resolution of the A/D converter was 0.6 mV. The voltages proportional to the lift and drag forces were acquired along with a voltage proportional to the velocity at the entrance to the test section. The acquisition software was programmed to acquire 10,000 voltage samples over 10 s. This was found to provide repeatable time averaged statistics that varied by less than 0.1%.

The angular position of the airfoil was controlled by voltage pulses from the DIO into the stepper motor controller. With this, the angular position was repeatable to within ± 0.005 deg. A mechanical readout that was geared to the stepper motor shaft provided positive feedback on the angular position.

Before making lift–drag measurements, values of the lift and drag voltages were first acquired at different angles of attack without flow. Any difference from the zero force voltage that was due to eccentric loading was then recorded and subtracted from the results at the same angles of attack with flow. This process was repeated anytime the model was removed from the force balance.

The freestream speed at the entrance to the measurement section was measured with a pitostatic probe connected to a pressure transducer. The output of the transducer was monitored on a dc volt meter and simultaneously acquired by the data acquisition computer when the voltages proportional to the lift and drag forces were acquired. Based on the pressure transducer calibration, the accuracy of the freestream speed measurements was 0.01 m/s. The combination of the uncertainties in the force measurements and velocity resulted in an average error in the lift and drag coefficients of approximately 1%.

B. Airfoil

The airfoil used in this study was a NACA 0015. This generic shape was chosen because its steady characteristics are well known and documented in the literature. This airfoil was also the subject of an experiment on the control of dynamic stall using plasma actuators [13–15,22], which provided flow visualization records.

The airfoil had a 12.7 cm (5 in.) chord and a 30.48 cm (12 in.) span. The size of the airfoil was a balance between minimizing blockage effects, especially at the large angles of attack that were investigated, and maintaining a large-enough chord Reynolds number to minimize stall hysteresis in the speed range for the facility. At the largest angle of attack of 23 deg, the solid blockage was 8.5%, which still ultimately required correction for the blockage in the measured lift

and drag coefficients. The method of correction was based on the practices in AGARD Report 109 [23] to account for blockage effects in the linear lift versus angle of attack range, before stall. It combined the effects of the solid blockage at a zero angle of attack, E_{sb_0}, the solid blockage at incidence angles, E_{sb}, and the wake blockage, E_{wb}, where

$$E_{sb_0} = (\pi/6)(1 + 1.2(t/c))(A/(hw)) \tag{2}$$

$$E_{sb} = E_{sb_0}(1 + 1.1(c/t)(\alpha^2)) \tag{3}$$

and

$$E_{wb} = 0.25(c/h)C_{d_u} \tag{4}$$

In these expressions, t is the maximum airfoil thickness, A is the cross-sectional area of the airfoil, h and w are the height and width of the tunnel measurement section, and C_{d_u} is the uncorrected coefficient of drag. The total blockage is

$$E = E_{sb} + E_{wb} \tag{5}$$

Streamline curvature produced by the blockage is given as

$$\sigma = \pi^2/(48(c/h)^2 \tag{6}$$

The measured (subscript m) values of the lift and drag coefficients were then corrected for blockage effects:

$$C_L = C_{L_m}(1 - \sigma - 2E) \tag{7}$$

$$C_D = C_{D_m}(1 - 3E_{sb} - 2E_{wb}) \tag{8}$$

and the corrected Reynolds number was

$$Re_c = Re_{c_m}(1 + E) \tag{9}$$

The airfoil was cast using an epoxy-based polymer in a two-piece mold. The mold was precisely machined using a numerical-controlled milling machine. Photographs of the airfoil are shown in Fig. 4.

Two freestream speeds of 21 and 30 m/s were used in the experiments. The primary criterion for their selection was that the chord Reynolds number be above that value at which stall hysteresis was observed to occur. At these velocities, the chord Reynolds numbers are 180 and 257 K, which both satisfy our criterion. As a result of blockage, the corrected average Reynolds numbers for the two freestream speeds were 217 and 307 K.

C. Plasma Actuators

The plasma actuator consisted of two copper electrodes separated by two layers of 0.1-mm-thick (0.004-in.-thick) Kapton film. The electrodes were made from 0.0254-mm-thick copper foil tape. The electrodes were arranged in the asymmetric arrangement illustrated in Fig. 1. They were overlapped by a small amount (of the order of 0.5 mm), to ensure a uniform plasma in the full spanwise direction.

The plasma actuator was bonded directly to the surface of the airfoil. At the leading edge, where the flow is sensitive to the nose radius, a 0.2 mm recess was molded into the model to accept the actuator and produce a smooth, flush surface with the NACA 0015 airfoil shape. The bottom left and right photographs in Fig. 4b and 4c show the dark-colored Kapton sheet that fills this recess at the leading edge. The two copper foil electrodes were aligned in the spanwise direction. These were positioned so that the junction between the exposed and covered electrodes was precisely at the leading edge ($x/c = 0$). The asymmetric arrangement was oriented so that, at positive angles of attack, the covered electrode was on the suction side of the airfoil and the exposed electrode was on the pressure side. With this orientation, the actuator would induce a velocity component in the mean freestream direction over the suction surface of the airfoil. The actuator at the leading edge spanned the portion of

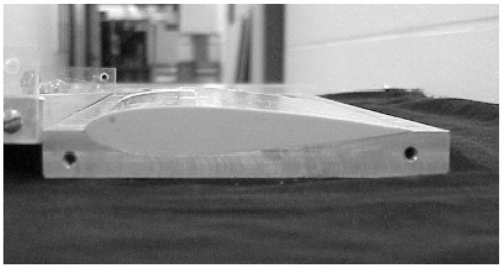

a)

b)

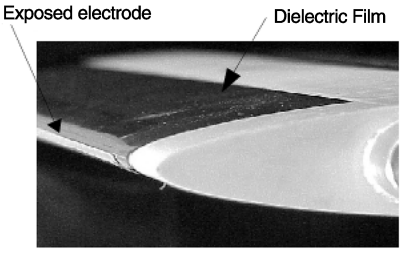

c)

Fig. 4 NACA 0015 airfoil model with plasma actuators used in experiment.

the width of the airfoil corresponding to the Kapton (dark) covering seen in Fig. 4b.

The trailing-edge actuator was located on the suction side of the airfoil for positive angles of attack at $x/c = 0.90$. This can be seen near the trailing edge of the airfoil in Fig. 4b. The design of the actuator is similar to that at the leading edge. It is oriented so that the exposed electrode is upstream of the covered electrode to induce a flow in the mean downstream direction. The junction between the exposed and covered electrodes is located at $x/c = 0.90$.

The two actuators were controlled individually. The operating frequency of the ac voltage supplied to the electrodes was typically from 3 to 5 kHz. The actual frequency was tuned to minimize the overall power in the actuator electronics. The ac voltage amplitude to the electrodes ranged from 7 to 11 kV_{p-p}. The power used by the actuator varied depending on if it was steady or unsteady operation. For steady operation, it was estimated to be 20 W/ft span. The power estimate was found by displaying the voltage and current at the electrode on separate channels of an oscilloscope. The current was measured with an inductive pickup. The voltage was measured with a high-voltage probe. The product of these was computed over small increments of the ac period and summed to give the period-integrated power for one ac cycle. No attempt was made to impedance match the actuator to the driving electronics or to subtract off any reflected power. As a result, the 20 W/ft span is expected to be a conservative estimate.

The unsteady operation is illustrated in Fig. 5. It consisted of cycling the ac voltage off and on with an unsteady period, T. The percentage of time (duty) within the period that the ac was on was controllable. For the unsteady actuator cases, a duty cycle of only 10% was found to be sufficient for leading-edge-separation control. Thus, in these cases, the power was only one-tenth that for steady actuation, or approximately 2 W/ft span.

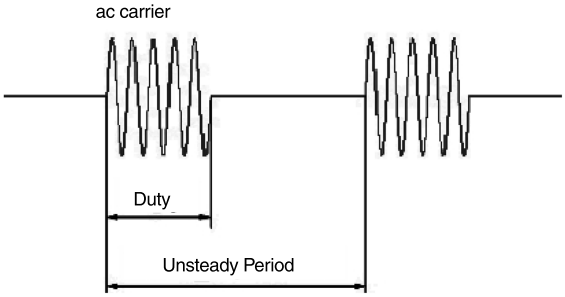

Fig. 5 Example of short duty cycle ac input for unsteady operation of plasma actuators.

Finally, care was taken to assure that the plasma actuators did not produce spurious errors in the voltage measurements. To verify this, the actuators were operated without flow. The voltages from the force balance were monitored on a digital oscilloscope. These showed no changes in the dc level or signs of electronic noise associated with the plasma actuator ac input.

III. Results

A. Leading-Edge Plasma Actuators (Plasma Slat Configuration)

Leading-edge-separation control effectiveness was evaluated on the basis of lift enhancement and drag reduction. The results presented here document the ability of the plasma actuators to reattach the flow over a stationary airfoil at high angles of attack, beyond natural static stall.

The lift and drag characteristics of the airfoil for the two freestream speeds with the plasma actuator off are presented in Figs. 6a and 6b, which shows the lift coefficient versus angle of attack (Fig. 6a) and the drag polar (Fig. 6b). The lift and drag coefficients have been corrected by accounting for the solid and wake blockage effects as discussed in the previous section. The linear theory slope, $dC_L/d\alpha = 0.11$, is shown for reference in the plot of C_L versus α. The good agreement is an indication that the results are consistent with thin airfoil theory.

For the drag polar, the drag of the wing support rod was not subtracted from the total drag. Therefore, the drag coefficients are larger than one would expect for this airfoil. However, the shape of the drag bucket in the linear lift region agrees well with archival results for this family of airfoils [24].

The characteristics of the airfoil are virtually identical at the two freestream speeds. The flow separates at an angle of attack of 14 deg. This is observed as a sharp decrease in lift and increase in drag. The degree of overlap in the coefficients at the two freestream speeds is also an indication of the accuracy of the force measurements.

Flow visualization was used to verify that the drop in lift at the large angles of attack was due to a separation of the flow at the leading edge. A sample of this taken from Post [13] is shown in Fig. 7a. For Figs. 7a and 7b, smoke streak lines were introduced in the contraction upstream of the test section at the spanwise centerline of the airfoil. Figure 7a shows the flow with the airfoil at a poststall of $\alpha = 16$ deg. This shows a large separation region that covers the total upper surface of the airfoil. Time-resolved observation of the separation region indicates it to be highly unsteady and with tracer material that is recirculating and well mixed.

Figure 7b shows the visualized flow when the leading-edge plasma actuator was on in steady operation. With the actuator on, the flow is observed to be attached all along the upper surface. The actuator conditions leading to this state at angles of attack above the natural stall angle are of particular interest.

With steady operation of the actuator, the only input parameter is the actuator amplitude needed to reattach the flow. We therefore examined this for different angles of attack. An example for $\alpha =$ 16 deg at the lower freestream speed is shown in Fig. 8. This documents the lift and drag coefficients normalized by their maximum values as a function of the actuator voltage that is normalized by a reference minimum value. The reference minimum

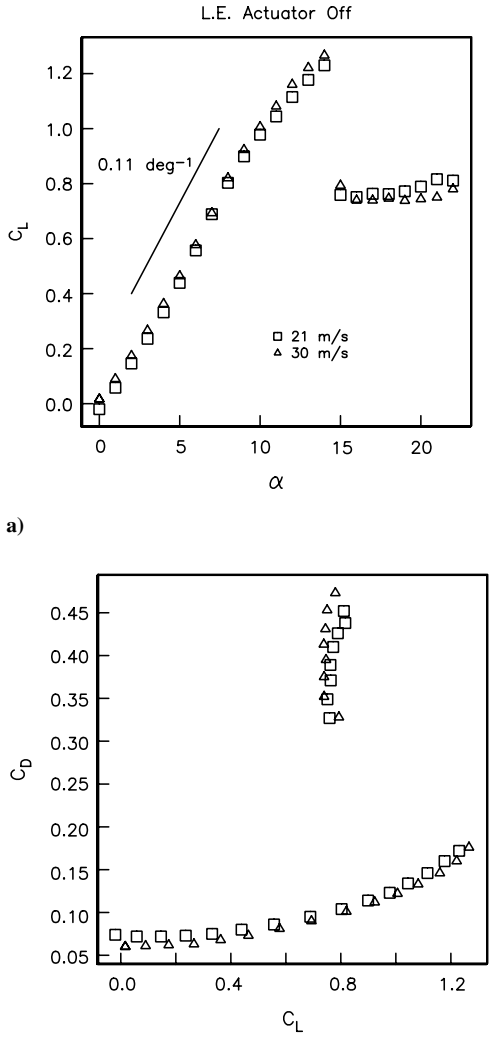

Fig. 6 Lift coefficient versus angle of attack and drag polar for the airfoil at both freestream speeds with the plasma actuator off.

voltage was 2.8 kV, which was sufficient to produce a plasma that was weakly visible in the darkened lab. The maximum lift coefficient, $C_{L_{\max}}$, used in the normalization was the blockage-corrected value at $U_\infty = 21$ m/s and $\alpha = 16$ deg equal to 1.25.

At $\alpha = 16$ deg, the flow over the airfoil was naturally separated and the lift coefficient was low and the drag coefficient was high. When the actuator voltages were too low, the flow remained separated and there was no improvement in the lift and drag. This corresponds to the left edge of the plot. However, once a threshold voltage to the actuator was reached, the flow dramatically reattached. This is observed as a large increase in the lift and decrease in the drag. The voltage condition at which this occurred is marked by the dashed line in the plot. Above this voltage, there was little change in the lift and drag coefficients.

Similar experiments were done for different angles of attack and the two freestream speeds. These were used to determine the voltage required to reattach the flow. The results are compiled in Fig. 9. Focusing first on the results for the higher velocity, the voltage required to reattach the flow was essentially independent of the angle of attack. This was also the case for the higher angles, $\alpha \geq 17$ deg, at the lower freestream speed. Therefore, based on these results, a single steady actuator voltage was selected that would assure that the flow would reattach at least up to $\alpha = 18$ deg. The selected voltage is indicated by the dashed line.

The result of the leading-edge actuators on the lift versus angle of attack and drag polar for the two freestream speeds is presented in Figs. 10 and 11. The data for the steady operation are shown as the

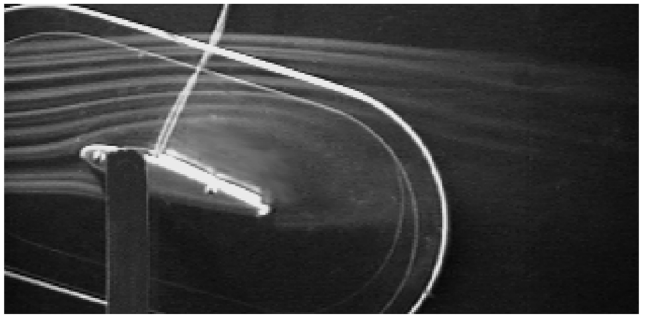

a)

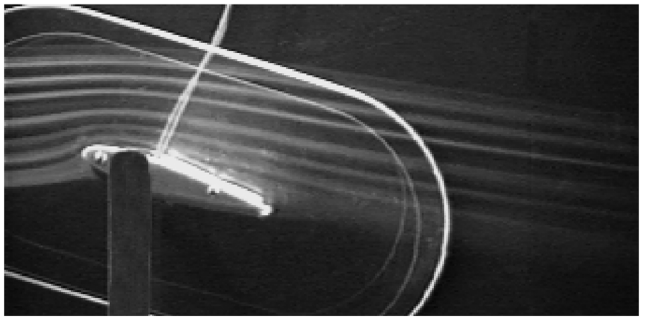

b)

Fig. 7 Visualized flow around airfoil at $\alpha = 16$ deg: a) leading-edge plasma actuator off, and b) on in steady operation [13].

circle symbols. At both freestream speeds, the steady actuation is observed to maintain lift up to $\alpha \simeq 18$ deg. In addition, the eventual drop in lift that occurs above this angle is more gradual than without the leading-edge flow control.

Also included in Figs. 10 and 11 are the results for the unsteady actuator operation. This is shown as the triangle symbols. As described earlier, the unsteady operation involves turning the actuator ac input on and off at a lower frequency (see Fig. 5).

It has been shown in the literature that the introduction of unsteady disturbances near the separation location can cause the generation of large coherent vortical structures that could prevent or delay the onset of separation. These structures are thought to intermittently bring high-momentum fluid to the surface, enabling the flow to withstand the adverse pressure gradient without separating. Periodic excitation by oscillatory blowing for use in separation control has been documented extensively by Seifert et al. [25] and in the review by Greenblatt and Wygnanski [26].

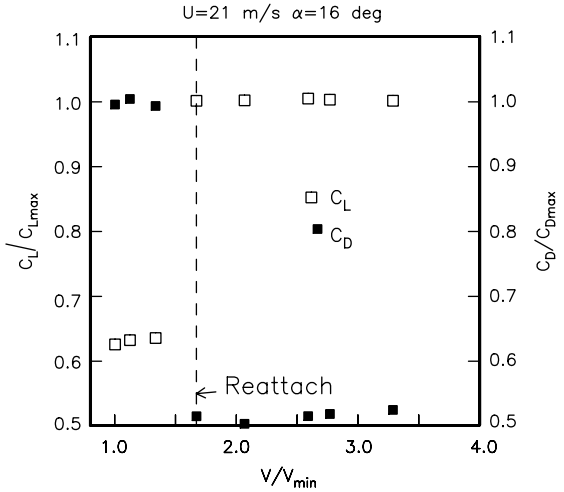

Fig. 8 Effect of the steady leading-edge plasma actuator voltage on the lift and drag coefficient for initially separated flow at $\alpha = 16$ deg. $V_{min} = 2.8$ kV.

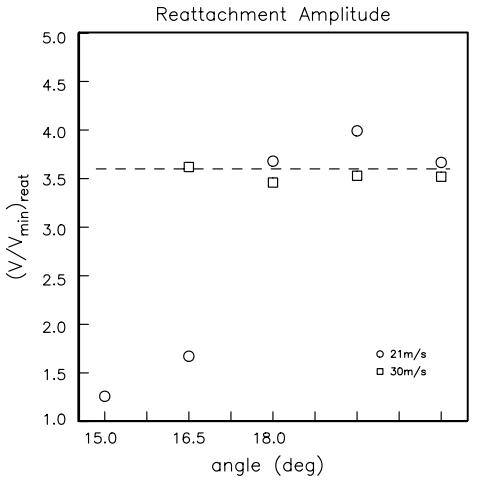

Fig. 9 Steady leading-edge plasma actuator voltage required to attach the flow for a range of angle of attacks and freestream speeds. $V_{min} = 2.8$ kV.

The forcing frequency for the unsteady disturbances is believed to be optimum when the Strouhal number, $St = fL_{sep}/U_\infty$, is near unity [25]. Here, f is the actuator forcing frequency; L_{sep} is the length of the separation zone, which, in this case with leading-edge separation, is the airfoil chord length c; and U_∞ is the freestream velocity. Table 1 lists the physical frequencies based on $St = 1$ for our conditions.

Included in Fig. 10 are curves that correspond to numerical simulations performed by Voikov et al. [27] of the flow over the

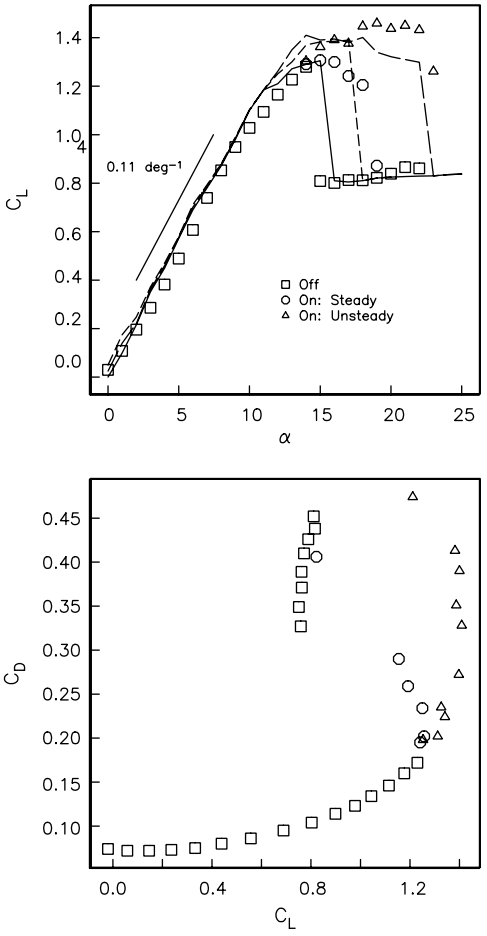

Fig. 10 Lift coefficient versus angle of attack and drag polar for the airfoil at 21 m/s. Curves are from numerical simulations [27].

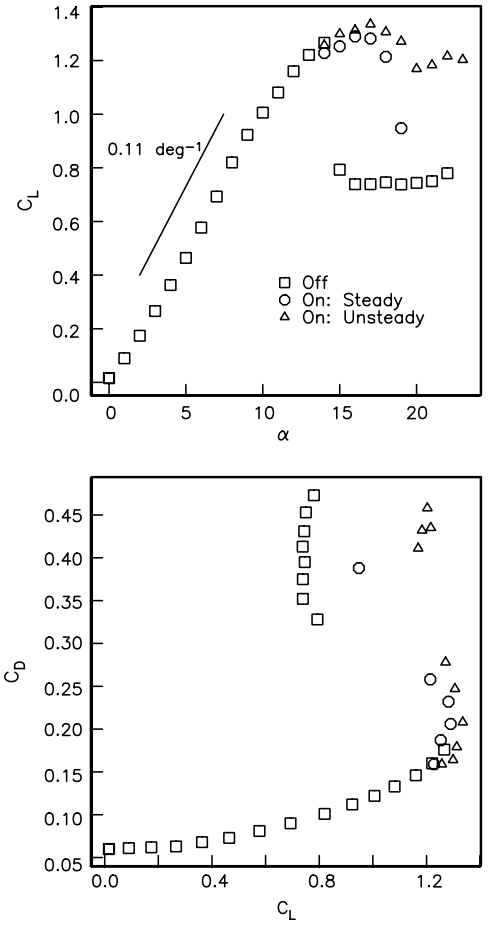

Fig. 11 Lift coefficient versus angle of attack and drag polar for the airfoil at 30 m/s.

airfoil that includes the body force produced by the plasma actuator. The simulation involved adding the body force distribution from the actuator into the momentum equation. The body force distribution comes from a numerical model developed by Orlov [6]. The simulation is time dependent, and the effect of the periodic actuation was included by turning the body force on and off at a specified interval in the computational time steps that corresponded to the optimum Strouhal number used in the experiment. The good agreement between the simulation and experiment validates the physical model for the SDBD plasma actuator.

A sensitivity study was performed to determine if an optimum frequency existed for the unsteady actuator in our case. This involved the airfoil at $\alpha = 16$ deg and $U_\infty = 21$ m/s. The results, presented in Fig. 12, show that a clear minimum in the voltage required to reattach the flow exists at an unsteady frequency that is close to that for which $St = 1$. This finding was then applied for the unsteady operation that gave the results in C_L and C_D in Figs. 10 and 11.

At both freestream speeds, the unsteady actuator at $St = 1$ gave significantly better results than the steady operation. At the lower freestream speed (Fig. 10), it significantly increased $C_{L_{\max}}$ and α_{stall} and maintained lift to $\alpha = 22$ deg, which was 7 deg past the natural stall angle of attack. Similar improvements were also found for the higher freestream speed. These results were obtained while using a 10% duty of the unsteady cycle. As a result, the power to the actuator

Table 1 Unsteady actuator frequencies for $St = 1$

U_∞, m/s	f, Hz
21	166
30	237

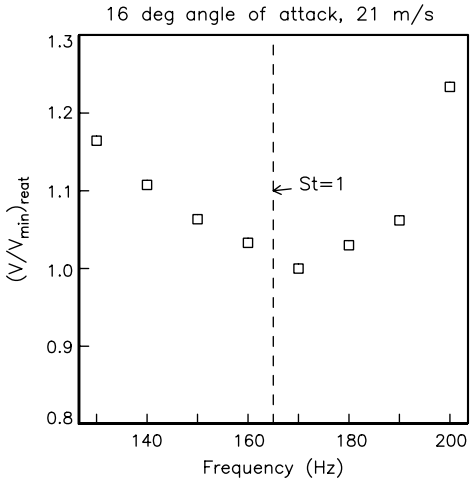

Fig. 12 Minimum voltage required to reattach flow versus actuator frequency for unsteady operation. $U_\infty = 21$ m/s, $\alpha = 16$ deg.

was only 10% that of the steady operation. The power in these cases was then only approximately 2 W.

We further compare the steady and unsteady actuation by examining the improvement they provide to the lift-to-drag ratios at high angles of attack. This is presented for the two freestream speeds in Figs. 13 and 14.

A substantial improvement in the lift-to-drag ratio was obtained with the leading-edge actuator at both freestream speeds. At its maximum, this ranged from approximately a 2.8 times improvement at the lower speed to approximately a 3.4 times improvement at the higher freestream speed.

Overall, the unsteady actuator produced a greater improvement that extended over a larger range of angles of attack. When this is factored with the 90% lower power required by the unsteady actuator, the system gains are substantially better.

B. Trailing-Edge Plasma Actuators (Plasma Flap Configuration)

This section presents results of operating a plasma actuator that was placed near the trailing edge of the airfoil at $x/c = 0.9$. The intention was to examine its ability to control the lift at angles of attack that were in the linear C_L versus α region. This follows a similar study by Corke et al. [10] that examined the effect of from one to four plasma actuators located between $x/c = 0.72$ and 0.9 on a NACA 0009 airfoil. The plasma actuators in that work were operated in the steady mode. There was no indication that unsteady operation used in flow separation control would affect the mean lift.

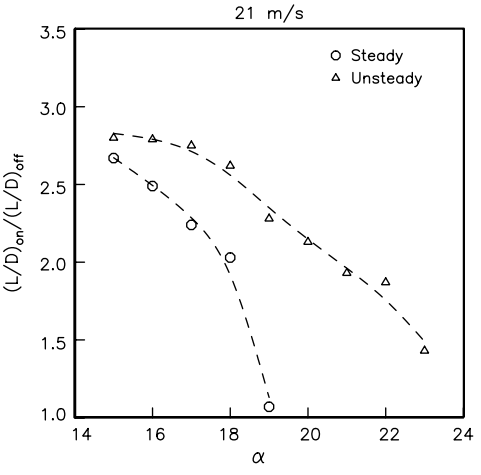

Fig. 13 Comparison of lift-to-drag ratio improvement for the steady and unsteady actuator at different angles of attack for $U_\infty = 21$ m/s.

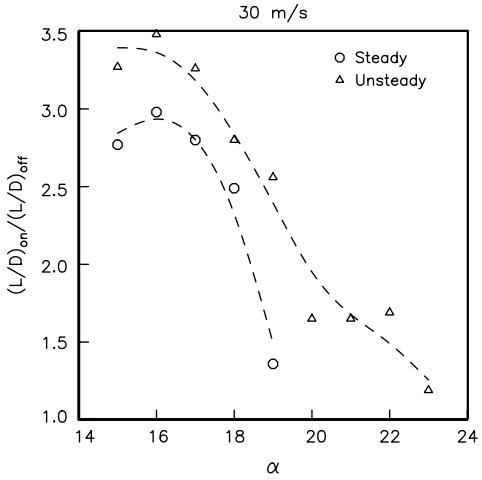

Fig. 14 Comparison of lift-to-drag ratio improvement for the steady and unsteady actuator at different angles of attack for $U_\infty = 30$ m/s.

As was shown in Fig. 4b, the plasma actuator spanned most of the suction side of the airfoil for positive angles of attack. The leading-edge actuator was not operated when investigating the trailing-edge actuator.

The lift coefficient versus angle of attack, and drag polar, with the trailing-edge actuator is presented in Fig. 15. This corresponds to the freestream speed of 21 m/s. The blockage-corrected chord Reynolds number in this case was 217 K, which was close to the 180 K value used in related experiments [10] in a facility at the U.S. Air Force Academy.

The solid curve corresponds to when the actuator was off. This represents the base condition for the airfoil. The dashed curve corresponds to the case with the actuator on in steady operation with an ac voltage amplitude of 7 kV_{p-p}.

As had been observed previously [10], the effect of the plasma actuator was to uniformly increase the lift coefficient at a given angle of attack. The change, ΔC_L, was approximately 0.051. This corresponded to an added lift force of 0.549 N (0.12 lb). For reference, this was 12% larger than that obtained by Corke et al. [10] with a slightly thinner (NACA 0009) airfoil. The applied voltage in that experiment was 5 kV, but the freestream velocity was somewhat lower at 15.2 m/s.

The drag polars in Fig. 15b indicate that the effect of the trailing-edge actuator is to shift the drag bucket to the right, that is, in the direction of higher C_L. There was also a slight decrease in the minimum drag coefficient. This is in contrast to the previous work [10], in which the single actuator at $x/c = 0.72$ resulted in an increase in the minimum drag coefficient.

The increase in lift and shift of the drag bucket toward higher C_L that was produced by the actuator is identical to the behavior of a plain trailing-edge flap. Thus, we have termed this a "plasma flap." Note that this behavior does not occur if the actuator is operated in the unsteady manner. The obvious advantages of this approach are that, for simplicity, there are no moving parts and there is no hinge gap that adds drag.

Using a plain flap as a model, we can estimate the effective flap deflection that gives the same amount of shift in the zero-angle lift coefficient, $\Delta_{\alpha_{0L}}$. The estimate was based on a 2-D NACA 0015 wing section at Mach 0.1 with a plain flap with $c_f/c = 0.1$. For a plain flap, the value of $\Delta_{\alpha_{0L}}$ comes from

$$\Delta_{\alpha_{0L}} = -\frac{\mathrm{d}C_l}{\mathrm{d}\delta_f}\frac{K'}{C_{L_\alpha}}\delta_f \tag{10}$$

where C_{L_α} is the 2-D section left coefficient (nominally 2π rad^{-1}), and K' is a correction for nonlinear effects that is a function of c_f/c and δ_f. The value of K' can be found in Fig. 8.3 of Corke [1]. For $c_f/c = 0.1$ and small flap deflections, $\delta_f \leq 10$ deg, the nonlinear effects are minimal and $K' = 1$.

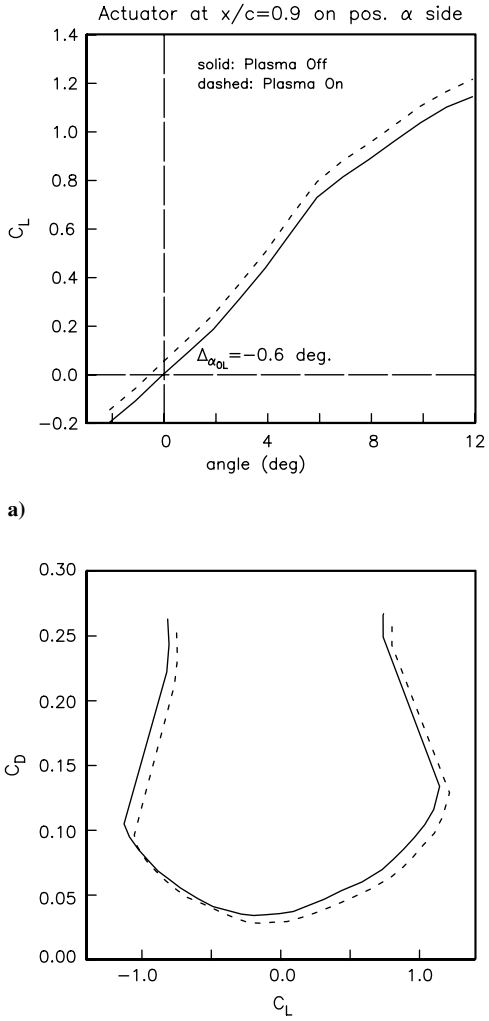

Fig. 15 Lift coefficient versus angle of attack and drag polar for the airfoil at 21 m/s: a) trailing-edge plasma actuator off, and b) trailing-edge plasma actuator steady on at 7 kV_{p-p}.

From the experimental results shown in Fig. 15b, $\Delta_{\alpha_{0L}} = -0.6$ deg. This corresponds to an equivalent plain flap deflection of $\delta_f = 1.5$. Even for this nominally small actuator voltage, the equivalent plain flap deflection is in the range of aileron deflections used for flight corrections during cruise, which is where we expect this to be most applicable.

IV. Discussion

A. Separation Control

The experiments demonstrated the ability of a SDBD plasma actuator at the leading edge to substantially increase the stall angle of attack and lift-to-drag ratio at natural poststall conditions. The actuator design used in the experiment has been documented [13] to produce an effect similar to a wall jet. The arrangement at the leading edge oriented the actuator so that the jet effect would be toward the suction side of the airfoil at positive angles of attack.

The actuator was operated in steady and unsteady manners. Both of these were found to increase the stall angle of attack; however, besides using more power, the steady operation was less effective than the unsteady operation. The mechanism of the steady actuator is believed to be the redistribution of fluid momentum in the region with a strong adverse pressure gradient near the leading edge. The more-effective unsteady operation was believed to be producing coherent vortical structures that introduced added circulation near the leading edge. For the unsteady operation, an optimum frequency

was found such that $St = fc/U_\infty = 1$, where the chord length, c, is the characteristic length scale of the flow separation zone.

An unsteady frequency with $St = 1$ has been found to be optimum for separation control in a number of other applications using plasma actuators [13,20]. The significance of this frequency scaling can be seen by considering that the unsteady actuator produces periodic vortical structures that convect in the mean flow direction. For an unsteady frequency, f, the wave length between structures would be $\lambda = c_r/f$, where c_r is the convection speed. Substituting for frequency in the Strouhal number definition gives

$$St = fL_{\text{sep}}/U_\infty = (c_r L/\lambda U_\infty) = 1 \tag{11}$$

The nominal convection speed of a large-scale vortical structure in a boundary layer is $c_r \simeq 0.5U_\infty$. Therefore, upon substitution,

$$\lambda = 0.5L_{\text{sep}} \tag{12}$$

Based on this scaling, we would expect that the mechanism for the optimum separation control that occurs at $St = 1$ would be to maintain a pair of vortical structures in the space of the separated region. The existence of such vortical structures was revealed in flow visualization by Huang et al. [20] for trailing-edge-separation control using a plasma actuator on a simulated turbine blade. They found that the unsteady actuator was only effective when it was oriented to induce a wall flow in the external mean flow direction. This is consistent with the concept that the actuator would produce vortical structures that were of the same sign as the mean vorticity in the boundary layer. The same mechanism is expected to occur in the leading-edge application in our experiments.

B. Trailing-Edge Plasma Actuators for Roll Control

The plasma actuator located near the trailing edge of the wing section was found to shift the lift coefficient in a manner that was similar to increasing the wing camber. Following the initial experiments, numerical simulations of the steady plasma actuator effect on lift enhancement on airfoils was done by Hall [28] and Hall et al. [29]. This involved an inviscid panel method model in which the plasma actuator was simulated as a doublet. The similarities in the flow effects of the plasma actuator and inviscid doublet were first demonstrated by Orlov et al. [7]. The simulations investigated the effects of the number, placement, and amplitude of actuators on the lift coefficient for a range of angles of attack within the linear dC_l/d_α range. The simulations were found to capture all the results of this and the previous experiment. In particular the simulations indicated that actuators placed nearer to the trailing edge produced a larger ΔC_L than those placed nearer to the leading edge. Multiple actuators operated together had an additive effect on ΔC_L.

The following paragraphs investigate the potential for the use of the plasma actuators to replace moving aileron surfaces for roll control on aircraft. Figure 16 shows an illustration of a plasma actuator arrangement on a rectangular wing with wing span b and chord c. The plasma actuators have a length L_a. One actuator would be located on the upper surface and the other would be on the lower surface. For the symmetric airfoil used in this study at a positive angle of attack, the upper surface actuator would produce an increase in lift and the lower surface actuator would produce a decrease in the lift over the affected wing area, S_a. The result would be a positive roll

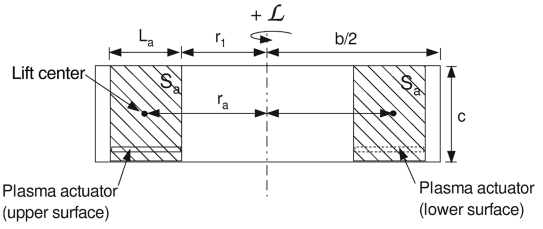

Fig. 16 Illustration of pair of plasma actuators used for roll control on a 2-D wing.

Table 2 Wing characteristics for Navion general aviation aircraft [30].

Characteristic	Value
$b/2$	5.07 m
c_{mean}	1.58 m
r_a	3.37 m
L_a	1.49 m
$C_{\mathcal{L}_{\delta a}}$	0.155 rad^{-1}

moment, $\mathcal{L}$. Assuming, for simplification, that the lift force is uniform in span over the area S_a, the magnitude of the roll moment is

$$\mathcal{L} = 2(\Delta C_L) q S_a r_a \tag{13}$$

The roll moment coefficient is

$$C_{\mathcal{L}} = \frac{\mathcal{L}}{qS_w b} = \frac{2(\Delta C_L) S_a r_a}{S_w b} \tag{14}$$

where S_w is the wing area used in normalization. The moment arm r_a is the distance from the spanwise center of lift to the roll axis location.

To provide some values for the magnitude of the roll moment coefficient that could be produced by plasma actuators, we consider for reference a Navion general aviation aircraft [30]. Table 2 summarizes the important dimensions.

Assuming that the moving ailerons were replaced by plasma actuators on the Navion, substituting values from Table 2, one obtains $C_{\mathcal{L}} = 0.0061$. Based on the value of roll moment derivative $C_{\mathcal{L}_{\delta a}}$ in Table 2 for the Navion, $C_{\mathcal{L}} = 0.0061$ produced by the plasma actuators would be equivalent to the roll moment coefficient on the Navion that results from an aileron deflection of $\delta_a = 2.5$ deg. This is certainly a respectable value. If one considers placing plasma actuators along the full wing span, then $C_{\mathcal{L}} = \Delta C_L/2$. In the case of the plasma actuator in this experiment, $C_{\mathcal{L}} = 0.026$. Then the equivalent aileron deflection for the Navion aircraft for this condition is $\delta_a \simeq 9$ deg, which is a very respectable control authority for roll.

The voltages used in the trailing-edge plasma actuator in this case were relatively low. However, it is known [2,4,13] that the body force produced by the actuator on the ambient flow increases in proportion to the applied voltage to the 7/2 power. Therefore, small increases in the voltage over those used in this experiment will produce larger effects. Thus, it is possible to further improve the roll moment authority of the actuator in the example discussed.

V. Conclusions

The experiment examined the use of plasma actuators at the leading edge to control separation and at the trailing edge to control lift. At the leading edge, the actuator was operated in both a steady and unsteady manner. The steady actuator was able to reattach the flow for angles of attack up to 18 deg, which was 4 deg past the normal stall angle. Even better performance was found with unsteady actuation, which was able to reattach the flow up to 8 deg past the normal stall angle. An optimum unsteady actuation frequency corresponding to $St = fL_{\text{sep}}/U_\infty = 1$ was used in these cases, where $L_{\text{sep}} = c$ for the leading-edge separation. The power to the actuator in these cases was approximately 2 W.

The leading-edge-separation control resulted in an increase in both $C_{L_{\max}}$ and α_{stall}. It resulted in an L/D improvement of as much as 340%.

The trailing-edge actuator was located on the surface of one side of the airfoil at $x/c = 0.90$ and spanned most of its width. When operated in a steady manner, it was found to produce the same effect as a plain trailing-edge flap. This included a uniform shift at all angles of attack of the lift coefficient and a shift toward higher C_L of the drag bucket. In addition, there was a slight decrease in the minimum C_D. An example of their use as ailerons for roll control produced a roll moment coefficient comparable to a sample general aviation aircraft.

Acknowledgment

This work was supported by a subcontract from Orbital Research, Inc., in support of the Small Business Innovation Research Phase I Contract No. F33615-03-M-3327. The program manager was Charles Suchomel. The U. S. Government is authorized to reproduce and distribute reprints for government purposes not withstanding any copyright notation therein.

References

[1] Corke, T. C., *Design of Aircraft*, Prentice–Hall, New York, 2002, pp. 38–59.

[2] Enloe, L., McLaughlin, T., VanDyken, R., Kachner, K., Jumper, E., and Corke, T., "Mechanisms and Response of a Single Dielectric Barrier Plasma Actuator: Plasma Morphology," *AIAA Journal*, Vol. 42, No. 3, 2004, pp. 589–594. doi:10.2514/1.2305; also AIAA Paper 2003-1021.

[3] Corke, T. C., Post, M. L., and Orlov, D. M., "SDBD Plasma Enhanced Aerodynamics: Concepts, Optimization and Applications," *Progress in Aerospace Science*, Vol. 43, Nos. 7–82007, pp. 193–217. doi:10.1016/j.paerosci.2007.06.001

[4] Enloe, L., McLaughlin, T., VanDyken, R., Kachner, K., Jumper, E., Corke, T., Post, M., and Haddad, O., "Mechanisms and Response of a Single Dielectric Barrier Plasma Actuator: Geometric Effects," *AIAA Journal*, Vol. 42, No. 3, 2004, pp. 589–594. doi:10.2514/1.2305

[5] Orlov, D., Corke, T., and Patel, M., "Electric Circuit Model for Aerodynamic Plasma Actuator," AIAA Paper 2006-1206, Jan. 2006.

[6] Orlov, D., "Modelling and Simulation of Single Dielectric Barrier Discharge Plasma Actuators," Ph.D. Dissertation, University of Notre Dame, Notre Dame, IN, 2006.

[7] Orlov, D., Erturk, E., Post, M., and Corke, T., "DNS Modeling of Plasma Array Flow Actuators," *Bulletin of the American Physical Society Fluid Dynamics Division*, Archives of the Bulletin of the American Physical Society, College Park, MD, 2001, http://www.aps.org/meetings/baps/index.cfm.

[8] Orlov, D., Corke, T., and Post, M., "DNS Modeling of Plasma Array Flow Actuators," *Bulletin of the American Physical Society Fluid Dynamics Division*, Archives of the Bulletin of the American Physical Society, College Park, MD, 2002, http://www.aps.org/meetings/baps/index.cfm.

[9] Orlov, D., Corke, T., and Haddad, O., "DNS Modeling of Plasma Actuators," *Bulletin of the American Physical Society Fluid Dynamics Division*, Archives of the Bulletin of the American Physical Society, College Park, MD, 2003, http://www.aps.org/meetings/baps/index.cfm.

[10] Corke, T., Jumper, E., Post, M., Orlov, D., and McLaughlin, T., "Application of Weakly-Ionized Plasmas as Wing Flow-Control Devices," AIAA Paper 2002-0350, Jan. 2002.

[11] Patel, M., Ng, T., Vasudevan, S., Corke, T., and He, C., "Plasma Actuators for Hingeless Aerodynamic Control of an Unmanned Air Vehicle," *Journal of Aircraft*, Vol. 44, No. 4, 2007. doi:10.2514/1.25368

[12] Lopera, J., Ng, T., Patel, M., Vasudevan, S., Santavicca, E., and Corke, T., "Aerodynamic Control Using Windward-Surface Plasma Actuators on a Separation Ramp," *Journal of Aircraft*, Vol. 44, No. 6, 2007. doi:10.2514/1.30741

[13] Post, M., "Plasma Actuators for Separation Control on Stationary and Oscillating Wings," Ph.D. Dissertation, University of Notre Dame, Notre Dame, IN, 2004.

[14] Post, M., and T. Corke, "Separation Control on High Angle of Attack Airfoil Using Plasma Actuators," *AIAA Journal*, Vol. 42, No. 11, 2004, p. 2177. doi:10.2514/1.2929

[15] Post, M., and Corke, T., "Separation Control Using Plasma Actuators: Dynamic Stall Control on an Oscillating Airfoil," *AIAA Journal*, Vol. 44, No. 12, Dec. 2006.

[16] Patel, M., Ng, T., Vasudevan, S., Corke, T., Post, M., McLaughlin, T., and Suchomelm, C., "Scaling Effects of an Aerodynamic Plasma Actuator," *Journal of Aircraft*, Vol. 45, No. 1, 2008. doi:10.2514/1.31830

[17] Hultgren, L., and Ashpis, D., "Demonstration of Separation Delay with Glow-Discharge Plasma," AIAA Paper 2003-1035, Jan. 2002.

[18] List, J., Byerley, A., McLaughlin, T., and VanDyken, R., "Using Plasma Actuator Flaps to Control Laminar Separation on Turbine Blades in a Linear Cascade," AIAA Paper 2003-1026, Jan. 2003.

[19] Huang, J., Corke, T. C., and Thomas, F. O., "Plasma Actuators for Separation Control of Low Pressure Turbine Blades," *AIAA Journal*, Vol. 44, No. 1, 2006, pp. 51–58. doi:10.2514/1.2903

[20] Huang, J., Corke, T. C., and Thomas, F. O., "Unsteady Plasma Actuators for Separation Control of Low Pressure Turbine Blades," *AIAA Journal*, Vol. 44, No. 7, 2006, pp. 1477–1487. doi:10.2514/1.19243

[21] Mueller, T. J., "Aerodynamic Measurements at Low Reynolds Numbers for Fixed Wing Micro Air Vehicles," *Development and Operation of UAVs for Military and Civil Applications*, Canada Communications Group, Inc., Quebec, Canada, April 2000, pp. 8-1–8-32.

[22] Post, M., "Phased Plasma Actuators for Unsteady Flow Control," M.S. Thesis, University of Notre Dame, Notre Dame, IN, 2001.

[23] Garner, H., Rogers, E., Acum, E., and Maskell, C., *Subsonic Wind Tunnel Wall Corrections*, AGARDograph 109, AGARD, Neuilly-sur-Seine, France, Oct. 1966.

[24] Abbott, I., and Von Doenhoff, A., *Theory of Wing Sections*, Dover, New York, 1949.

[25] Seifert, A., Darabi, A., and Wygnanski, I., "Delay of Airfoil Stall by Periodic Excitation," *Journal of Aircraft*, Vol. 33, No. 4, 1996, pp. 691–698. doi:10.2514/3.47003

[26] Greenblatt, D., and Wygnanski, I., "The Control of Separation by Periodic Excitation," *Progress in Aerospace Sciences*, Vol. 36, 2000, pp. 487–545. doi:10.1016/S0376-0421(00)00008-7

[27] Voikov, V., Corke, T., and Haddad, O., "Numerical Simulation of Flow Control over Airfoils Using Plasma Actuators," *Bulletin of the American Physical Society Fluid Dynamics Division*, Archives of the Bulletin of the American Physical Society, College Park, MD, 2004, http://www.aps.org/meetings/baps/index.cfm.

[28] Hall, K. D., "Potential Flow Model for Plasma Actuation as a Lift Enhancement Device," M.S. Thesis, University of Notre Dame, Notre Dame, IN, 2004.

[29] Hall, K., Jumper, E., Corke, T., and McLaughlin, T., "Potential Flow Model of a Plasma Actuator as a Lift Enhancement Device," AIAA Paper 2005-0783, 2005.

[30] Nelson, R., *Flight Stability and Automatic Control*, 2nd ed., McGraw–Hill, New York, 1998, pp. 83–84.